MOF-reduced Graphene Oxide Composites with Enhanced Electrocatalytic Activity for Oxygen Reduction Reaction

Yuan Zhao[1], Rong Fan[1], Chuanxiang Zhang[2], Haijun Tao[1], Jianjun Xue[1]
1 College of Material Science and Science Technology, Nanjing University of Aeronautics and Astronautics, Nanjing 211106, PR China
2 College of Materials Engineering, Nanjing Institute of Technology, Nanjing 211167, PR China
E-mail: zy871817440@163.com

Abstract. Development of inexpensive and scalable cathode catalysts that can efficiently catalyze the oxygen reduction reaction (ORR) is of significance in practical application of fuel cells. The oxygen reduction activity of the MOF-based catalyst is much lower than that of Pt, which is mainly due to the high overpotential. In this work, we designed a superior composite named Co@Co_3O_4-reduced graphene oxide (Co@Co_3O_4-rGO) derived from MOF-rGO by an in-situ synthetic method which gathered both the advantages of MOF and rGO. The Co^{2+} which belongs to the MOF provides the metal source, while the N sources are supplied by the organic ligands benzimidazole. With the combination of rGO, Co@Co_3O_4-rGO has got a higher specific surface area and much better transport pathways for oxygen and the electrolyte than Co@Co_3O_4-C derived from the pure MOF. The half-wave potential, onset potential of Co@Co_3O_4-rGO are close to the superior commercial Pt/C catalyst. The number of electron transfer in the process of catalytic oxygen reduction is close to 4, the excellent properties benefited from the synergistic effect of rGO and MOF.

1. Inrtoduction

Global resource shortages and environmental pollution have forced us to seek alternative energy conversion and storage systems with the advantages of high efficiency, low cost and environmental benignity [1]. With these advantages, Direct Methanol Fuel Cells (DMFC) has been concerned widely, the oxygen reduction reaction (ORR) is one of the most basically and the core technology of electrochemical reactions for DMFC [2]-[4]. Generally, Pt-based nanomaterials have been applied on promoting the oxygen reduction reaction as catalysts for their dominant electro-catalysts. Nevertheless, resource starvation, high price, poor stability and environmentally hazardous hinders Pt-based catalysts being widely applied to practical application in fuel cell devices. To overcome these bottlenecks, non-precious metal-based nanomaterials electro-catalysts have been intensively studied for substituting the high cost electro –catalysts Pt for the oxygen reduction reaction [5]-[8].

Metal-organic frameworks (MOFs) are built from the reaction of metal ions and organic ligands, which have the advantage of particular porous structures and high specific surface area [9]-[11]. It has caught attention of plenty of researchers in gas adsorption[12]-[14], storage [15-17], sensors [10] and catalysis [18], [19]. Moreover, zeolitic imidazolate framework (ZIFs) could be designed with abundant metal-N_x coordinate moieties that can improve electro-catalytic performance [20]. As a result, most

MOF-derived electrocatalysts for ORR were based on porous carbon materials prepared by pyrolysis of ZIFs or ZIF-supported precursors [18]. Unfortunately, the oxygen reduction activity of the MOF-based catalyst is much lower than that of Pt, which is mainly due to the high overpotential effect of the MOF-based catalyst, which can be divided into two vital aspects. On the one hand, nitrogen-doped carbon or M-N-C structure which supplies active sites plays a vital role on ORR catalysts but not effective. On the other hand, the transmission of O_2 and the interaction between electrolytes with catalysts are limited .In this regard, in order to obtain more efficient catalysts for ORR, the most vital factor is how to get rapid mass transport properties of ordered carbon nanomaterials [21]. Graphene, a two-dimensional sheet of sp^2 conjugated carbon atoms, can be considered as a giant polyaromatic platform for performing chemistry due to its open ended structure [21], [22]. The combination of high specific surface area and high electrical conductivity makes graphene sheets high promising as an electrocatalyst platform. Loh et al.[23] studied the electro-catalytic action of the composites of MOFs and graphene oxide (GO) on the hydrogen evolution reaction (HER), oxygen evolution reaction (OER), and oxygen reduction reaction (ORR). Their studies showed that the composites exhibited the better electrochemical performance and stability than that of pure MOFs due to the synergistic effect of GO and MOF. Therefore, in-depth study of MOF-graphene composites is necessary.

In this work, we report a ZIF9-based nanomaterial which was inserted into reduced graphene oxide by an in situ method. In the process of Benzimidazole and $Co(NO_3)_2 \cdot 6H_2O$ were used as precursors to synthesis ZIF9, at the same time reduced graphene oxide was added into the mixture, MOF-rGO composite was obtained in one step. Then after thermal treatment under the atmosphere of N_2, $Co@Co_3O_4$-rGo composite was synthesized finally. During the prepared composite is pyrolyzed into $Co@Co_3O_4$-rGO, the Co^{2+} which was surrounded by benzimidazole ligands converted into $Co@Co_3O_4$ and it was wrap by N-doped porous carbon derived from benzimidazole. And the rGO can enhancing the electron transfer between metal oxide nanoparticles and carbon support. Due to the improvement mentioned above, the $Co@Co_3O_4$-rGO which prepared showed higher ORR catalyst performance than $Co@Co_3O_4$,which is approach to the commercial Pt/C catalyst. And the $Co@Co_3O_4$ -rGO electrocatalyst also revealed excellent stability and methanol tolerance in comparison to the Pt/C catalyst at the same time.

2. Experiment

2.1. Synthesis of MOF-rGO

Graphite oxide(GO) was prepared by oxidation of graphite powder via modified Hummers' method [24]. The reduced graphene is obtained by hydrazine hydrate reduction [25]. In order to obtain the MOF-rGO, $Co(NO_3)_2 \cdot 6H_2O$ (0.42g,1.44 mmol) was dissolved into DMF(20 mL), 0.1g r-GO was added to the solution above and sonicated for 30 min. In other hand, benzimidazole (0.17 g) was dissolved into 30 mL DMF, and this solution was stirred for 10 min. Then reflux unit was equipped, and the vessel was heated at 130 ℃ for 12 h. After cooling to room temperature the as-formed MOF-rGO composite was obtain by filtration and washed with water and ethanol several times. The filter residue was dried by freeze-drying.

2.2 Synthesis of $Co@Co_3O_4$ and $Co@Co_3O_4$-rGO

The above prepared MOF and MOF-rGO composite was added into porcelain crucible and then pyrolyzed at 800 ℃ for 2 h under the atmosphere of Ar_2 before cooling down to room temperature. The composite was heated to 500℃ at a heating rate of 10℃ min^{-1}, then obtained material was heated to 800℃ at a heating rate of 5℃ min^{-1}. At last, via thermal treatment the purple MOF and atropurpureus MOF-rGO composite was converted to black powder.

2.3 Characterization

The crystal structure of the electro-catalyst was identified by X-ray diffraction (XRD) 2θ ranges from 10 °to 90 °. X-ray spectroscopy (XPS) was performed by. The morphological structure of the electro-catalyst was investigated by scanning electron microscopy measurements and transmission electron

microscopy. Raman spectra were characterized by Micro-Raman Spectroscopy System (Renishaw inVia).

2.4 Electrochemical measurements

All the electrochemical measurements were carried through CHI660D electrochemical workstation which was supplied by CHENHUA Shanghai via a standard three-electrode system. The working electrode was a glassy carbon rotating disk electrode (GC) which was coated by the catalyst with a diameter 5 mm. First, the working electrode was polished by α-Al_2O_3 powders in order to get a smooth, neat and clean surface, and then washed with deionized water and ethanol before using. To prepare the working electrode,5mg of the as-prepared electro-catalyst which was prepared with different doping content and different calcination temperature and 50 μ L Nafion solution were mixed and dispersed in 1mL 1:4 (v/v) water/ethanol mixed solvent and the mixture were treated with sonication for 1h at least in order to obtain a homogeneous suspension solution. The 20% Pt/C catalyst was also prepared by the method mentioned above. Then 25 μ L of the mixed suspension were dropwise added onto the surface of the GC electrode and dried in air with natural drying. An Hg/Hg_2Cl_2 electrode with KCl solution was used for reference electrode and Pt sheet was applied as counter electrode. All potentials here are converted to a reversible hydrogen electrode (RHE) scale.

Cyclic voltammetry (CV) and linear sweep voltammetry (LSV) were performed in a N_2-saturated and an O_2-saturated 0.1 M KOH in the potential range of 0-1.2 V (*vs*. RHE). All the electrochemical measurements were performed in a 0.1 mol/L KOH aqueous solution which was used as electrolyte at room temperature with pumping oxygen or nitrogen into the electrolyte.

Koutechy-Levich equation.

$$\frac{1}{J}=\frac{1}{J_L}+\frac{1}{J_K}=\frac{1}{B\omega^{1/2}}+\frac{1}{J_K} \tag{1}$$

$$B=0.2nFC_0(D_0)^{2/3}v^{-1/6} \tag{2}$$

Here J represents the measured electric current density, J_L and J_K are the diffusion and kinetic-limiting electric current densities, respectively. ω means the angular velocity , n is the electrons number which was transferred during the ORR, F is faraday constant (96485 C mol^{-1}) , C_0 is the bulk concentration of O_2 in 0.1 M KOH (1.26×10^{-3}mol L^{-1}), D_0 is the oxygen diffusion coefficient in 0.1 M KOH (D_0 = 1.9×10^{-5} cm^2 s^{-1}) and V is the kinetic viscosity of the electrolyte (n=0.01cm^2 s^{-1}). Chronoamperometric measurements were also performed in an O_2-saturated KOH electrolyte adding the methanol with the purpose of testing the methanol tolerance performance of the electro-catalyst [26].

3. Results and discussion

Morphological and microstructure were investigated by scanning electron microscopy (SEM) and transmission electron microscopy (TEM). As shown in fig 1a, the pure MOF have got a purple appearance, respectively. However, the MOF-rGO composite in fig.1c displays a comprehensive appearance between purple and black which can defined as modena. The morphologies and structural features of the as-prepared electro-catalyst, including MOF, rGO and Co@Co_3O_4-rGO can be observed clearly and directly from SEM and TEM images. SEM images of the pure MOF and MOF-rGO are shown in fig.2b and fig.2d. As we can see from fig.2d, a layer of rGO with parts of drapes tiled in the image.Fig.2b displays the nubbly morphology of the pure MOF, fig.2d reveals the nubbly MOF was inserted into the carbon layer of rGO forming MOF-rGO. MOF-rGO was pyrolyzed under N_2 atmosphere in order to prepare Co@Co_3O_4-rGO, as it is shown in fig.2e, the rGO is still remained via thermal treatment and Co@Co_3O_4 nanopaticles are uniformly distributed and anchored in the layer of rGO.

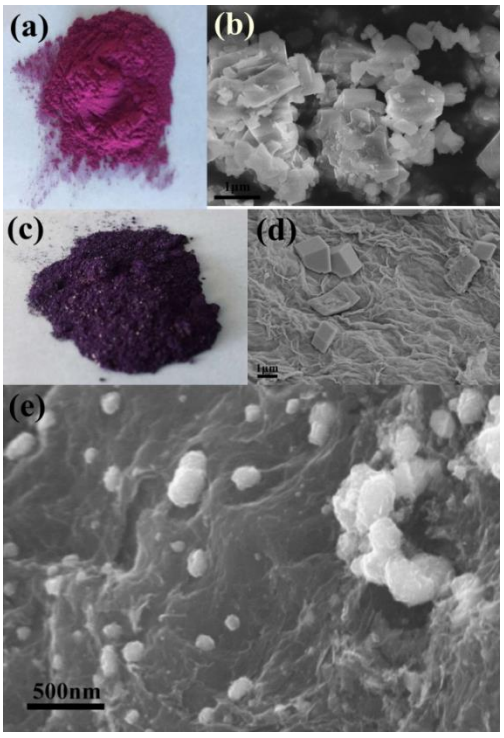

Figure 1. Photographs of (a) ZIF9 (c) ZIF9-rGO; SEM images of (b) ZIF9, (d) ZIF9-rGO and (e) Co@Co_3O_4-rGO

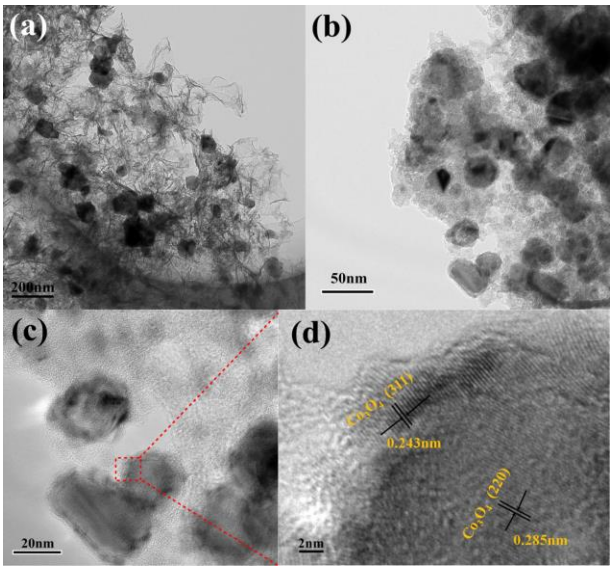

Figure 2. TEM image of (a) ZIF9-rGO, and (b) Co@Co_3O_4-rGO. HRTEM images of (c) (d) Co@Co_3O_4-rGO

The tulle-like graphene can be seen in the TEM spectrum clearly (fig 2(a)), after high temperature pyrolysis, the graphene transition to C, and Co^{2+} that exists in the layer is also converted into Co_3O_4. As shown in fig 2(d) the high-resolution TEM (HRTEM) image reveals that the lattice spacings of Co_3O_4 nanocrystala on rGO are 0.243nm and 0.285nm, and which mathes well with the lattice spcings of Co_3O_4 (311) and (220). This result is consistent with the XRD spectrum.

In order to further analyze the structure and chemical composition of the Co@Co_3O_4-rGO composites, XRD and XPS analysis were performed.. From fig 3a, the characteristic peaks of Co, Co_3O_4, C can be observed obviously. The prominently sharp carbon peak at 26.2° came from the carbon which was pyrolyzed from benzimidazole after combined with rGO. The peak at 44.3° is assigned to the (111) lattice plane of Co, also the peaks at 51.3° and 76.2° are assigned to the (200) and (220) lattice plane Co_3O_4 respectly. The lattice planes mentioned above further testify the existence of Co. The rest peaks corresponding to the (111),(220),(311),(511) and (440) lattice planes [27].

The full XPS spectrum of the Co@Co_3O_4-rGo fig.3b demonstrates the existence of the element of carbon, cobalt, nitrogen and oxygen. Among the elements mentioned above, the nitrogen element is derived from the benzimidazolate ligands. We can see from the high-resolution XPS spectrum of N peaks, pyridinic N (398 eV), pyrrolic N (400 eV) and graphitic N (401 eV) can be observed in fig.3c. Pyridine nitrogen can provide effective oxygen reduction activity site [28]. The regional Co 2p spectrum displayed in fig.3d indicates that there are two energy bands, the higher energy band is at 795 eV(Co $2p_{1/2}$), the lower one is at 780 eV(Co $2p_{3/2}$).

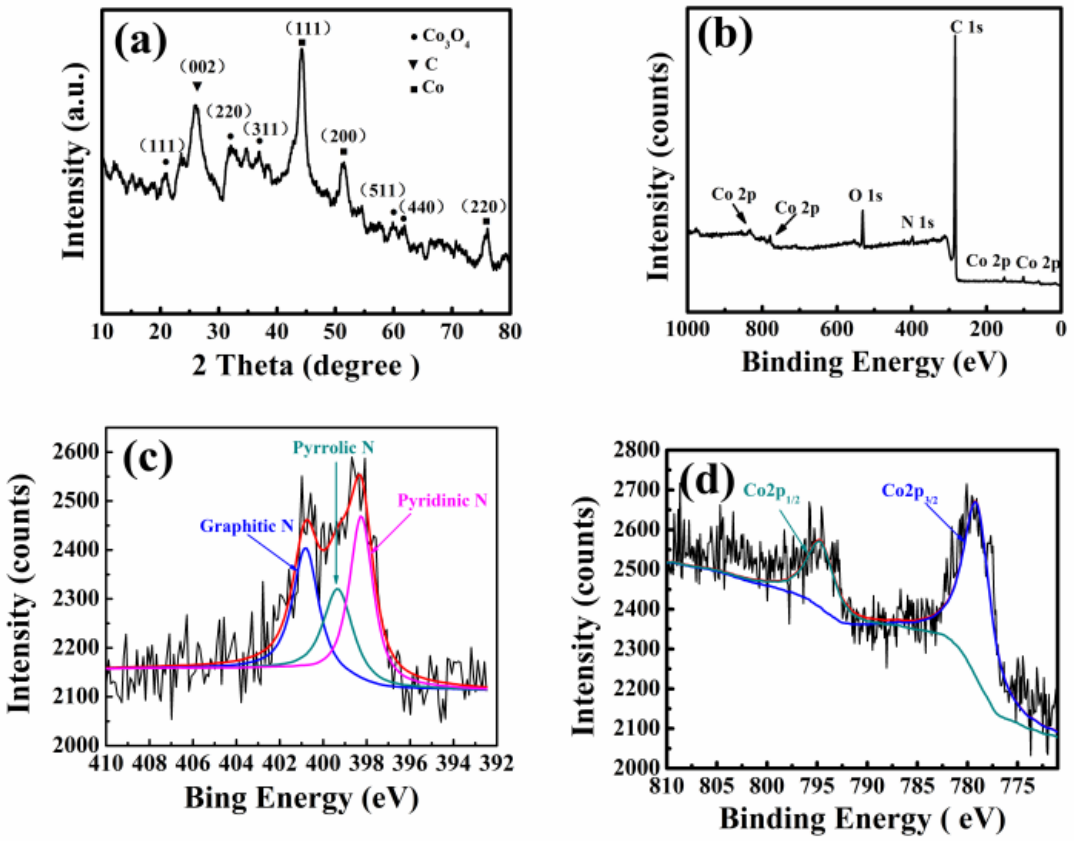

Figure 3. (a) XRD pattern, (b) XPS full spectrum, (c) N1s spectrum and (d) Co 2p XPS spectrum.

Co@Co_3O_4-rGO shows type IV isotherms (mesoprous capillart condensation) with a H3-type hysteresis loop (P/P_0 >0.4), indicating the nanocatalyst is a mesoprous. As we can see from the Fig 4b, MOF-rGO also shows type IV isotherms while it shows H4-type hysteresis loop. Also from the BJH method we obtained the pore size is about 4.36 nm and the Brunauer–Emmett–Teller (BET) surface area is 305.4 m^2g^{-1},as well as the cumulative pore volumes is 0.31cm^3g^{-1}. Contrasted to the pure MOF Fig 4a, the composite has much higher specific surface area. The results displayed upon demonstrated that the high surface areas and pores of the pyrolyzed pure MOF remained after thermal treatment. The pyrolyzed composite shows better ORR catalytic activity than the pyrolyzed pure MOF as a result of the improvement on specific surface area and pore size.

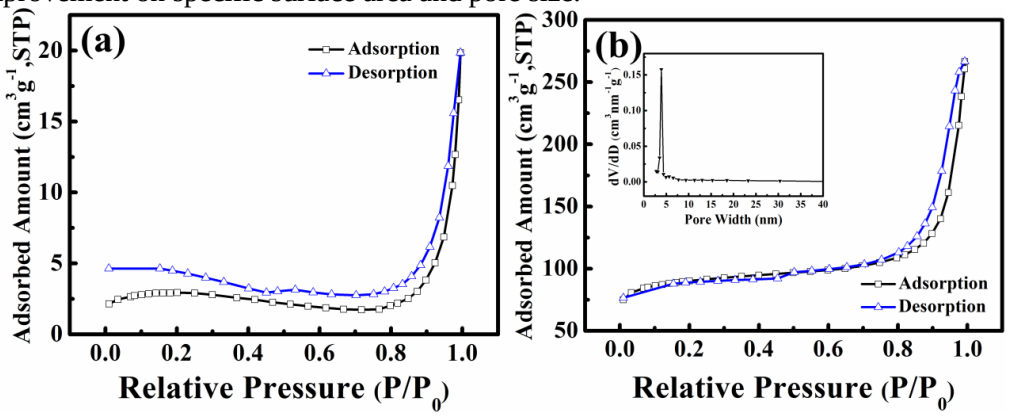

Figure 4. Nitrogen sorption isotherms of (a) ZIF9 and (b) Co@Co_3O_4-rGO composite.

The inset shows corresponding pore size distribution based on the Quenched Solid Density Functional Theory (QSDFT) model using the adsorption branch.

In electrochemical measurements section, the CV of $Co@Co_3O_4$-rGO catalyst take place in 0.1M KOH solution. As we can see from fig.5a, the $Co@Co_3O_4$-rGO catalyst shows a common curve with no characteristic in N_2-saturated solution. Nevertheless, the $Co@Co_3O_4$-rGO catalyst reveals obvious cathodic peaks for the ORR in O_2-saturated 0.1M KOH solution. The fig.5b displays the ORR polarization curves of $Co@Co_3O_4$-rGO,$Co@Co_3O_4$,rGO and commercial Pt/C via linear sweep voltammetry. It is not difficult to see that the catalysts obtained from MOF-rGO has got a higher onset potential of 0.90 V and a higher half-wave potential of 0.85 V than the catalyst derived from pure MOF with the onset potential of 0.84 V and the half-wave potential of 0.79 V. It is worth mentioning that the half-wave potential, onset potential of $Co@Co_3O_4$-rGO are close to the superior commercial Pt/C catalyst. As we can see from the comparison curves, the catalyst derived from composite material with the addition of rGO reveals obvious advantage on onset potential and limited current than the catalyst derived from the pure MOF. The rGO improves the electrical conductivity. In a word, the outstanding performance on ORR activity makes the $Co@Co_3O_4$-rGO be the most high-efficiency catalyst among the non-precious metal under the same loading capacity. In addition, the $Co@Co_3O_4$-rGO catalyst possesses a higher limit current density than that of $Co@Co_3O_4$ and the rGO, which is approaching to the limit current density of superior commercial Pt/C.

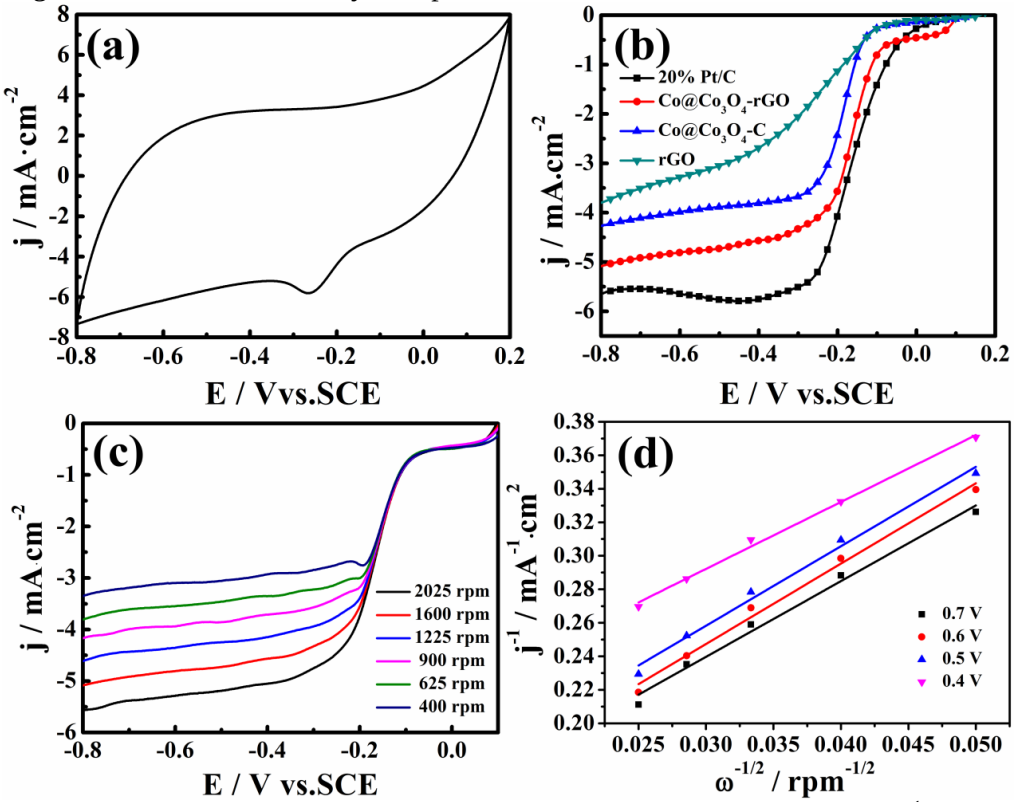

Figure 5. (a) Cyclic voltammograms of $Co@Co_3O_4$-rGO at a scan rate of 20mV s^{-1} in O_2-saturated aqueous solution of 0.1M KOH; (b)rotating disk electrode (RDE) voltammograms of 20% Pt/C, $Co@Co_3O_4$-rGO, $Co@Co_3O_4$-C, and rGO in an O_2-saturated 0.1M aqueous KOH solution with a scan rate of 5 mV s^{-1} at a constant rotation rate of 1600 rpm; (c) RDE voltammograms of $Co@Co_3O_4$-rGO at different rotation rates from 400 to 2025 rpm and (d) Koutecky-Levich plot for the electrode materials at -0.3V.

The linear sweep voltammetry curves at various rotating rates and corresponding Koutechy-Levich plots of $Co@Co_3O_4$-rGO are obtained and calculated which are shown in fig.5c and fig.5d. A good linearity of the plots and near parallelism of the fitting lines at various potentials were observed, suggesting that the reactions on $Co@Co_3O_4$-rGO are first-order over the potential range. To assess the ORR property of the catalysts fairly, the preferred electron transfer number should four[29]. As we obtained from the Koutechy-Levich calculation, the electron transfer number on $Co@Co_3O_4$-rGO

ranges from 3.8 to 3.9, which is very close to 4, indicating that the catalyst we synthesized suffers 4-electron during the ORR process.

4. Conclusions

In summary, this work offered an in situ method to prepare MOF-rGO by refluxing treatment of benzimidazole, cobaltous nitrate hexahydrate and reduced graphene oxide. And then after a step pyrolysis get Co@Co_3O_4-rGO directly. With the combination of rGO, Co@Co_3O_4-rGO has got a higher specific surface area and much better transport pathways for oxygen and the electrolyte than Co@Co_3O_4-C derived from the pure MOF. By analyzing the properties of as-obtained product, the Co@Co_3O_4-rGO catalyst demonstrated superior catalytic activity compared to Co@Co_3O_4-C and rGO. The excellent properties benefited from the synergistic effect of rGO and MOF. It is believed that the simple but efficient way could be further developed for the production of metal-free electrocatalyst to replace Pt/C in the area of fuel cell and metal-air battery in the future.

5. Acknowledgments

The authors gratefully acknowledge the Jiangsu Innovation Program for Graduate Education(Grant no. KYLX15-0305), Fundamental Research Fund for the Central Universities (Grant no.NS2015061), the Foundation of Graduate Innovation Center in NUAA (Grant no. KFJJ20160611), and Priority Academic Program Development of Jiangsu Higher Education Institutions for the financial support of this work.

6. References

[1] S. Chu and A. Majumdar, *Nature*, 2012, **488**, 294-303.
[2] S. K. Kamarudin, F. Achmad and W. R. W. Daud, *Int. J. Hydrogen Energy*, 2009, **34**, 6902-16.
[3] S. K. Kamarudin, W. R. W. Daud, S. L. Ho and U. A. Hasran, *J. Power Sources*, 2007, **163**, 743-54.
[4] R. Dillon, S. Srinivasan, A. S. Aricò and V. Antonucci, *J. Power Sources*, 2004, **127**, 112-26.
[5] M. Shao, Q. Chang, J. P. Dodelet and R. Chenitz, *Chem. Rev.*, 2016, 116, 3594-657.
[6] D. Li, H. Lv, Y. Kang, N. M. Markovic and V. R. Stamenkovic, *Annual Review of Chemical and Biomolecular Engineering*, 2016, 7, 509-32.
[7] J. Liu, P. Song, Z. Ning and W. Xu, *Electrocatalysis*, 2015, 6, 132-47.
[8] G. L. Tian, M. Q. Zhao, D. Yu, X. Y. Kong, J. Q. Huang, Q. Zhang and F. Wei, *Small*, 2014, **10**, 2251-59.
[9] W. Xia, J. Zhu, W. Guo, L. An, D. Xia and R. Zou, *J Mater Chem A*, 2014, **2**, 11606.
[10] L. E. Kreno, K. Leong, O. K. Farha, M. Allendorf, R. P. Van Duyne and J. T. Hupp, *Chem. Rev.*, 2012, **112**, 1105-25.
[11] J. L. C. Rowsell and O. M. Yaghi, *Microporous Mesoporous Mater.*, 2004, **73**, 3-14.
[12] C. Petit, B. Mendoza and T. J. Bandosz, *Langmuir*, 2010, **26**, 15302-9.
[13] X. Zhou, W. Huang, J. Shi, Z. Zhao, Q. Xia, Y. Li, H. Wang and Z. Li, *J Mater Chem A*, 2014, **2**, 4722.
[14] K. Sumida, D. L. Rogow, J. A. Mason, T. M. McDonald, E. D. Bloch, Z. R. Herm, T. H. Bae and J. R. Long, *Chem. Rev.*, 2012, **112**, 724-781.
[15] S. Liu, L. Sun, F. Xu, J. Zhang, C. Jiao, F. Li, Z. Li, S. Wang, Z. Wang, X. Jiang, H. Zhou, L. Yang and C. Schick, *Energ Environ Sci*, 2013, **6**, 818.
[16] Z. Li and L. Yin, *J. Mater. Chem. A*, 2015, **3**, 21569-77.
[17] D. Ji, H. Zhou, Y. Tong, J. Wang, M. Zhu, T. Chen and A. Yuan, *Chem. Eng. J.*, 2017, **313**, 1623-32.
[18] H. Wang, J. Wei, Y. Hu, Y. Liang, B. Kong, Z. Zheng, J. I. N. Zhang, S. P. Jiang and Y. Zhao, *J. Mater. Chem. A*, 2017, DOI: 10.1039/c7ta00276a.
[19] S. Ma, G. A. Goenaga, A. V. Call and D. J. Liu, *Chemistry*, 2011, **17**, 2063-7.
[20] W. Xia, R. Zou, L. An, D. Xia and S. Guo, *Energy Environ. Sci.*, 2015, **8**, 568-76.
[21] M. Jahan, Q. Bao and K. P. Loh, *J. Am. Chem. Soc.*, 2012, **134**, 6707-13.
[22] C. Huang, C. Li and G. Shi, *Energ Environ Sci*, 2012, **5**, 8848.

[23] M. Jahan, Z. Liu and K. P. Loh, *Adv. Funct. Mater.*, 2013, **23**, 5363-72.
[24] D. C. Marcano, D. V. Kosynkin, J. M. Berlin, A. Sinitskii, Z. Sun, A. Slesarev, L. B. Alemany, W. Lu and J. M. Tour, *ACS Nano*, 2010, **4**, 4806-14.
[25] D. Li, M. B. Muller, S. Gilje, R. B. Kaner and G. G. Wallace, *Nat Nanotechnol*, 2008, **3**, 101-5.
[26] W. N. Yan, X. C. Cao, J. H. Tian, C. Jin, K. Ke and R. Z. Yang, *Carbon*, 2016, **99**, 195-202.
[27] Y. Liang, Y. Li, H. Wang, J. Zhou, J. Wang, T. Regier and H. Dai, *Nat Mater*, 2011, **10**, 780-6.
[28] D. H. Guo, R. Shibuya, C. Akiba, S. Saji, T. Kondo and J. Nakamura, *Science*, 2016, **351**, 361-5.
[29] A. M. Gomez-Marin, R. Rizo and J. M. Feliu, *Catalysis Science & Technology*, 2014, **4**, 1685-98.